Florence, Italy 12-16 July 2015
ICSV22
The 22nd International Congress on Sound and Vibration

A STUDY OF ALIASING ERROR IN DGM SOLUTIONS TO TURBOFAN EXHAUST NOISE PROBLEMS

Michael Williamschen, Gwénaël Gabard
ISVR, University of Southampton, SO17 1BJ, Southampton, United Kingdom
email: m.williamschen@soton.ac.uk

Hadrien Bériot
Siemens PLM, Researchpark Z1, Interleuvenlaan 68, 3001, Leuven, Belgium

Highly non-uniform flows such as shear layers are an intrinsic feature of turbofan exhaust noise problems. Modeling the sound radiation from turbofan exhausts with the linearized Euler equations raises the issue of accurately representing strongly spatially-varying mean flows numerically, while ensuring that numerical solutions are not polluted by spurious solutions such as aliasing errors. This paper investigates the behavior of aliasing instabilities in time domain solutions obtained by the discontinuous Galerkin method. A model exhaust noise problem is studied to demonstrate the growth of unphysical temporal instabilities. A new fully-discrete dispersion analysis technique is developed that permits non-uniform mean flows. The dispersion analysis is used to study the spectral behavior of aliasing instabilities and the impact of polynomial order on their formation and growth. The results of this study indicate that aliasing errors are largely absolute instabilities which build up in the solution over time and are highly sensitive to the polynomial order.

1. Introduction

Accurately predicting the noise signature of turbofan exhausts is a challenging problem requiring a highly accurate solution scheme to resolve the disparate length and temporal scales, a model incorporating highly non-uniform mean flow effects such as strong shear layers, and a low computational cost to be useful as an engineering tool. The time domain, quadrature-free nodal discontinuous Galerkin method (DGM) [1] has proven to be a highly accurate and efficient solution scheme for aeroacoustics applications [2, 3, 4]. Applied to the linearized Euler equations (LEE), the LEE DGM can accurately and efficiently describe sound propagation through non-uniform mean flows and effects such as refraction, vorticity generation, and scattering of entropy and vorticity fluctuations into acoustic waves.

One challenge of solving the LEE is discretely representing the mean flow to ensure that the physical features of the flow are sufficiently described, while also ensuring that problem is well behaved numerically. This work focuses on the latter to demonstrate numerical issues, specifically aliasing, that can lead to unstable computations. The nodal DGM represents both the solution and the flux by polynomial interpolation. Aliasing error arises when the flux is composed of products of polynomials, and is then interpolated by a polynomial basis of a lower order than the product of the polynomials.

This interpolation essentially transforms higher order modes into lower order modes in the interpolated flux. Since the flux terms in the LEE consist of products of mean flow variables with the solution variables, aliasing error is introduced for non-uniform mean flows.

The aliasing problem is studied extensively in the spectral method community for non-linear problems [5], however little research has been done to investigate aliasing error arising in solutions to linear problems with non-uniform media. This paper investigates the aliasing problem specifically in application to the solution of the LEE with highly sheared mean flows by the DGM. A duct radiation problem with an artificially imposed shear layer is solved to illustrate aliasing instabilities. The spectral properties of aliasing are identified by solving a new, fully-discrete, dispersion analysis of the LEE DGM supporting non-uniform mean flows.

2. Governing equations and the numerical solution scheme

2.1 Linearized Euler equations in cylindrical coordinates

Sound propagation in a non-uniform, inviscid, fluid flow can be approximated by linearizing the conservative form of the three-dimensional Euler equations about a mean flow, resulting in the linearized Euler equations. For geometries with cylindrical symmetry, which is often the case for turbofan exhaust problems, it is convenient to work in the cylindrical coordinate system. A simplification to the problem can be made by performing a Fourier decomposition of the solution in the azimuthal direction,

$$\mathbf{q} = \sum_{m=-\infty}^{\infty} \mathbf{q}_m(r,x,t)e^{-im\theta}, \tag{1}$$

resulting in the three-dimensional formulation for each azimuthal mode, m, with derivatives in only two spatial dimensions,

$$\frac{\partial \mathbf{q}}{\partial t} + \frac{1}{r}\frac{\partial\left(\mathbf{F}_r\right)}{\partial r} - \frac{im}{r}\mathbf{F}_\theta + \frac{\partial\left(\mathbf{F}_x\right)}{\partial x} + \frac{1}{r}\mathbf{A}_c\mathbf{q} = \mathbf{S}, \tag{2}$$

where $\mathbf{q} = \left[\rho, \rho u_r, \rho u_\theta, \rho u_x, \pi\right]^{\mathrm{T}}$ is the vector of conserved variables and ρ, ρu_r, ρu_θ, ρu_x, and π are the fluctuating quantities of density, r-, θ-, and x-momentum, and a pressure ratio, $\pi = \left(\frac{p}{p_\infty}\right)^{\frac{1}{\gamma}}$, defined by Goldstein [6]. The term, $\mathbf{S}$, contains any sources present in the problem. The terms $\mathbf{F}_r = r\mathbf{A}_r\mathbf{q}$, $\mathbf{F}_\theta = \mathbf{A}_\theta\mathbf{q}$, and $\mathbf{F}_x = \mathbf{A}_x\mathbf{q}$ are flux terms in the r, θ, and x directions. The specific expressions for these matrices can be found in [7].

2.2 Time domain nodal quadrature-free DGM

Defining a triangular tessellation, $\Omega \subset \mathbb{R}^2$, an element, $D_k \in \Omega$, and requiring that the residual of Eq. (2) is orthogonal to all test functions $\phi \in \mathcal{L}$ in element D_k, where $\mathcal{L}_p = \{\phi_i, i = 1, \ldots, N_p\}$ is the space of Lagrange polynomials of order p,

$$\int_{D_k}\left(\frac{\partial \mathbf{q}^k}{\partial t} + \frac{\partial \mathbf{F}_r^k}{\partial r} + \frac{\partial \mathbf{F}_x^k}{\partial x} - \mathbf{S}\right)\phi_i \,\mathrm{d}D_k = 0, \quad 1 \le i \le N_p, \tag{3}$$

where $\mathbf{S}$ contains the source and the $\mathbf{F}_\theta$ and $\mathbf{A}_c\mathbf{q}$ terms. Integrating by parts twice, the strong formulation of the DGM becomes

$$\int_{D_k}\frac{\partial \mathbf{q}_k}{\partial t}\phi_i \, r\mathrm{d}D_k = \int_{D_k}\mathbf{S}_k\phi_i - \left(\frac{\partial \mathbf{F}_r^k}{\partial r} + \frac{\partial \mathbf{F}_x^k}{\partial x}\right)\phi_i \, r\mathrm{d}D_k + \sum_{b=1}^{3}\int_{\Gamma_{b,k}}\left(\mathbf{F}^{n,b} - \mathbf{f}^{n,b}\right)\phi_i \, r\mathrm{d}\Gamma_{b,k}, \tag{4}$$

where $\mathbf{F}^{n,b}$ is the flux normal to the edge b of element k, and $\mathbf{f}^{n,b}$ is a normal numerical flux through edge b of element k, which is chosen as the upwind flux in this work. The term, $\mathbf{S}_k$, contains products of the solution with the matrices, $\mathbf{A}_\theta$ and $\mathbf{A}_c$. The solution is defined through the interpolation at nodes on an element,

$$\mathbf{q} \approx \sum_{j=1}^{N_p} q_j(r_j, x_j, t)\phi_j(r, x), \tag{5}$$

where N_p is the number of points on the element, and q_j are the nodal solution values. Substituting Eq. (5) into the strong formulation, Eq. (4), the semi-discrete formulation becomes

$$\frac{\mathrm{d}\mathbf{q}^k}{\mathrm{d}t} = \mathbf{M}_k^{-1}\left[\mathbf{M}_k\mathbf{S}^k - \left(\mathbf{S}_r^k\mathbf{F}_r^k + \mathbf{S}_x^k\mathbf{F}_x^k\right) + \sum_{b=1}^{3}\mathbf{M}_k^b\left(\mathbf{F}_k^{n,b} - \mathbf{f}_k^{n,b}\right)\right], \tag{6}$$

where $\mathbf{M}$, $\mathbf{S}_r$, $\mathbf{S}_x$, and $\mathbf{M}_k^b$ are the mass, stiffness, and edge matrices, respectively.

Rather than compute the element matrices and store them for each element, the quadrature-free approach developed by Atkins and Shu [1] maps each triangular element to a reference element and requires storage of only the transformation Jacobian. This scheme allows for potentially large savings in computational cost as compared to traditional DGM. However, the element matrices for the cylindrical formulation have an explicit r-dependence and can not readily be mapped to a reference element. One solution is solve for $r\mathbf{q}$ rather than $\mathbf{q}$, but this raises the issue of recovering the solution on the axis, $r = 0$. To avoid these issues, the standard DGM is used to solve for $\mathbf{q}$ in all elements touching the axis, and the quadrature-free DGM is used to solve for $r\mathbf{q}$ in all other elements. The solution in the quadrature-free elements is divided by r when it is transferred to a neighboring non-quadrature-free element. The semi-discrete form of the LEE DGM above is integrated in time with the low-storage, six-stage Runge-Kutta scheme by Berland *et. al* [8] with fourth order temporal accuracy.

2.2.1 Aliasing

The flux terms in Eq. (6) involve products of the solution variables, a polynomial of order p, with mean flow variables. If the mean flow is a polynomial of order m, then the flux is a polynomial of order at least $p + m$. Interpolation of the flux with a polynomial of order p, transforms the higher order modes into lower order modes in the interpolated flux. This leads to the formation of aliasing errors which may degrade the solution and cause unphysical instabilities especially when using large elements with high polynomial orders [9]. Reducing the accuracy of the mean flow representation or applying a modal filter may reduce the aliasing errors, but at a possible cost of solution accuracy.

3. Fully-discrete dispersion analysis

To investigate the formation of aliasing-driven instabilities for the DGM, a fully-discrete dispersion analysis technique is developed. Other dispersion analyses of the DGM consider only model scalar equations on infinite-periodic meshes [10]. In this work, the dispersion analysis technique is similar to the dispersion analysis of a finite-difference scheme developed by Gabard and Brambley [11]. Consider the semi-infinite channel computational domain shown in Figure 1a, with uniform mesh spacing in the x and y directions, Δx and Δy. Assuming solutions of the LEE with the form, $\mathbf{q} \sim e^{i(\omega t - kx)}$, the solution at the boundary of the $n+1$-th element can be written in terms of the solution at the n-th boundary as $\mathbf{q}_{n+1} = \mathbf{q}_n e^{-ik_x\Delta x}$, where k_x is the wavenumber in the axial direction and $\mathbf{q}$ is the vector of nodal solution values of fluctuating density, momentum, and pressure ratio, concatenated with all elements in the mesh as $\mathbf{q} = \left[\mathbf{q}_1, \mathbf{q}_2, \ldots, \mathbf{q}_{N_k}\right]^{\mathrm{T}}$, with N_K defined as the total number of elements.

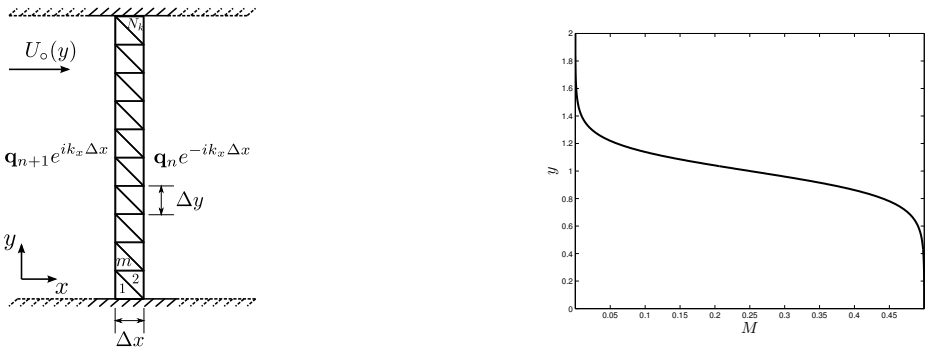

(a) (b)

Figure 1: Construction of a fully-discrete dispersion analysis (a) and the Mach number profile considered (b).

By enforcing periodicity only in the axial direction and leaving the transverse direction fully discretized, both non-uniform mean flow and mesh effects can be considered by the model. In this work, the hyperbolic-tangent mean flow Mach number profile illustrated in Figure 1b is imposed. Boundary conditions specific to the problem may be defined on the edges of the $m = 1$ and $m = N_K$ elements, such as hard walls, impedance surfaces, or absorbing layers. The dispersion analysis problem can be assembled into the following semi-discrete matrix form,

$$\frac{\mathrm{d}\mathbf{q}}{\mathrm{dt}} = \mathbf{M}^{-1}\begin{bmatrix} \mathbf{E}_{1,2} & \boldsymbol{\Sigma}_3^{p+1} & \mathbf{0} & \dots & \mathbf{0} \\ \boldsymbol{\Sigma}_2^{p-1} & \mathbf{E}_{3,4} & \boldsymbol{\Sigma}_5^{p+1} & \dots & \mathbf{0} \\ \vdots & & \ddots & & \vdots \\ \mathbf{0} & \dots & \mathbf{0} & \boldsymbol{\Sigma}_{N_k-2}^{p-1} & \mathbf{E}_{(N_k-1),N_k} \end{bmatrix}\mathbf{q}, \tag{7}$$

which is a block-tridiagonal matrix. The mass matrix, $\mathbf{M}$, is a block-diagonal matrix, containing each element's mass matrix. The flux term corresponding to degrees of freedom (DOF) on a two-element patch, $p = n, n+1$, is $\mathbf{E}_{n,n+1}$, and the contribution to the edge flux terms from DOF outside of patch p are $\boldsymbol{\Sigma}_n^{p-1}$ and $\boldsymbol{\Sigma}_n^{p+1}$. After replacing the time derivative with a low-storage Runge-Kutta scheme, the formulation becomes

$$e^{i\omega\Delta t}\mathbf{q} = \left[\mathbf{I} + \sum_{s=1}^{N_s}\gamma_s\left(\mathbf{A}\Delta t\right)^s\right]\mathbf{q}, \tag{8}$$

which is in the form of a generalized eigenvalue problem. The number of stages and the coefficients of the Runge-Kutta scheme are defined as N_s and γ_s, respectively. Solutions of Eq. (8) are in the form of $5 \times N_k \times N_p$ eigenvalues, $e^{i\omega\Delta t}$, which represent the growth of the solution modes over one time step, Δt, and eigenvectors, $\mathbf{q}$, which contain the solution at the nodal points. Solutions to Eq. (8) form a dispersion relation, $D(\omega, k) = 0$, numerically describing the time-evolution of the initial conditions. Only a few of the solution modes correspond to actual physical modes, the rest can be considered to be spurious.

4. Properties of the instabilities

This section applies the dispersion analysis technique developed above to a model shear layer problem. Numerical solutions to a duct radiation problem with an artificial shear layer are used to illustrate the behavior of aliasing-driven numerical instabilities in a problem with many similar features to a turbofan exhaust noise problem.

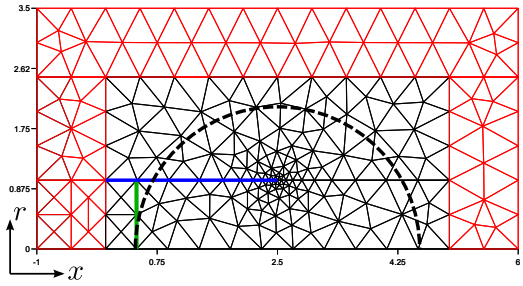

Figure 2: Computational setup of the duct radiation problem.

4.1 Semi-infinite axisymmetric duct problem

Consider the computational domain shown in Figure 2. A semi-infinite, zero thickness, hard wall duct with an exit plane at $x = 2.5$ is colored with a blue line. Duct modes are injected into the domain within the duct along the green line and the waves are allowed to leave the domain cleanly through the buffer regions, shown in red. The numerical and analytical solutions are compared on the black dashed line.

4.1.1 Verification

To verify the axisymmetric implementation, solutions to the duct radiation problem are performed and compared with the near-field analytical solutions developed by Gabard and Astley [12]. Only a single solution is shown in this work for brevity. A duct mode with a free-field wavenumber of $k_0 = 20$, azimuthal order 5, and radial order 0 is injected into a quiescent mean flow. Elements with a polynomial order, $p = 6$, are used. Figure 3a shows contours of fluctuating pressure after 60 periods of oscillation. The acoustic waves can be seen smoothly exiting the domain through the buffer region, outlined in black lines, with no noticeable reflections. Pressure, radial velocity, and axial velocity fluctuations are compared to the analytical solution in Figure 3b. Good agreement with the analytical solution is demonstrated for all solution variables.

4.2 Aliasing instabilities in the shear layer

Shear layers with strong gradients are a common feature of the mean flow in a turbofan exhaust noise problem. Consequently, these strong mean flow gradients can amplify the aliasing problem. To model this effect, the duct radiation problem in Section 4.1 is updated to include an artificially-imposed shear layer from the exit lip of the duct. The shear layer Mach number profile is given

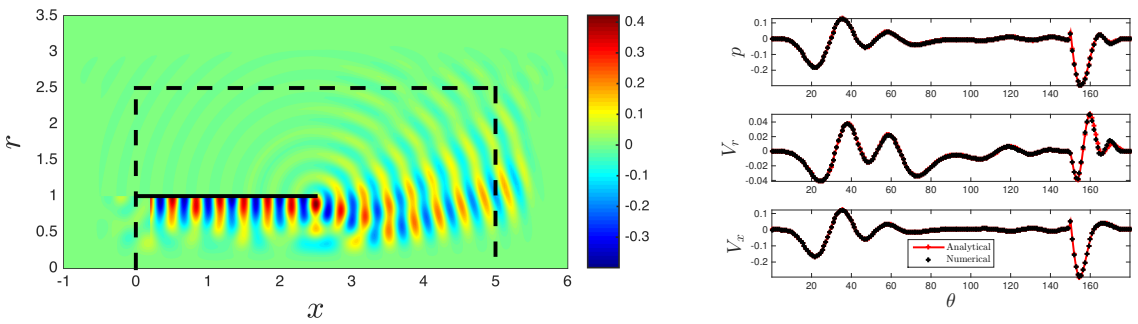

(a) (b)

Figure 3: Contours of pressure fluctuations (a) and a verification of the duct radiation problem (b).

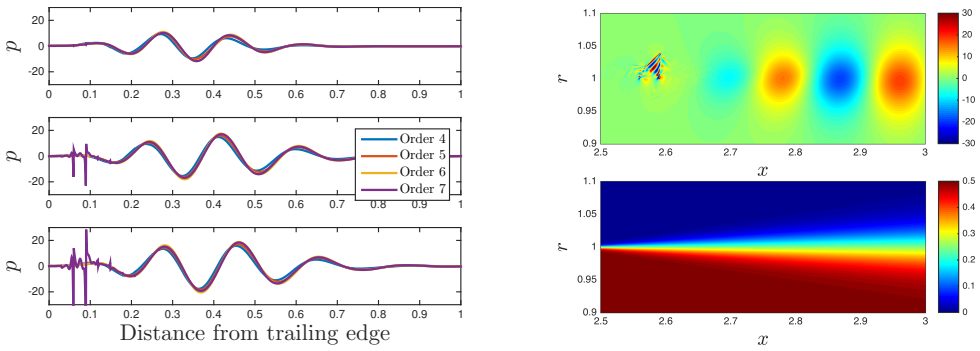

(a) (b)

Figure 4: Pressure fluctuations at consecutive times (a) and contours showing aliasing and the mean Mach number at the final time (b).

by

$$M = \frac{1}{4}\left(1 + \tanh\left[\frac{R}{2w}\left(1 - \frac{|r|}{R}\right)\right]\right), \tag{9}$$

where R is the duct radius and w is the shear layer thickness which varies in the x-direction as $w = 0.2(x - 2.45)\sin(\phi)$, with ϕ being the spreading angle. This mean velocity profile is imposed directly on the DGM nodes, and therefore with the same order polynomial representation as the solution variables.

A duct mode with a free-field wavenumber of $k_0 = 8.5$, azimuthal order 5, and radial order 0 is injected into the duct in the same manner as in Section 4.1.1. The shear layer region of the mesh is refined enough to resolve the hydrodynamic fluctuations and to accurately describe the strong mean flow gradients. As the solution evolves in time, the presence of a mean flow allows vorticity to be generated downstream of the duct lip. These vortices cause strong fluctuations in pressure downstream of the duct as shown in the top image in Figure 4a. The bottom two images show the pressure fluctuations at two subsequent times. For the polynomial order 7 solution, an unphysical instability forms and rapidly grows to a similar magnitude as the stable solution. Magnified images of the pressure contours at a time step of 10800 and the mean flow Mach number are shown in Figure 4b. It is clear that the instability is highly unphysical and is localized to a region with strong mean flow gradients.

4.3 Spectral analysis

4.3.1 Duct with a shear layer problem

Taking the spatial Fourier transforms of the pressure computed in Section 4.2 at times $t = 10800\Delta t$ and $t = 11000\Delta t$, the power spectrums are shown in Figure 5a. The range of wavenumbers, $k = 18$ to $k = 50$, represents the physical solution mode, with small growth from one time to the next. Outside of the physical region, there is a large growth over the time period and over a wide range of wavenumbers. From the ratio of two spectra, a solution growth rate, $-\mathrm{Im}(\omega)$, is calculated and shown in Figure 5b. The fast growth of the unphysical modes seen in Figure 4a is evident considering the large growth rates over the spectrum.

4.3.2 Dispersion analysis of wave propagation in a shear layer

The dispersion analysis developed in Section 3 can be used to study the error and stability properties of the LEE DGM for wave propagation through a sheared mean flow. While the physical problem in the dispersion analysis is fundamentally different than that of the duct radiation problem analyzed

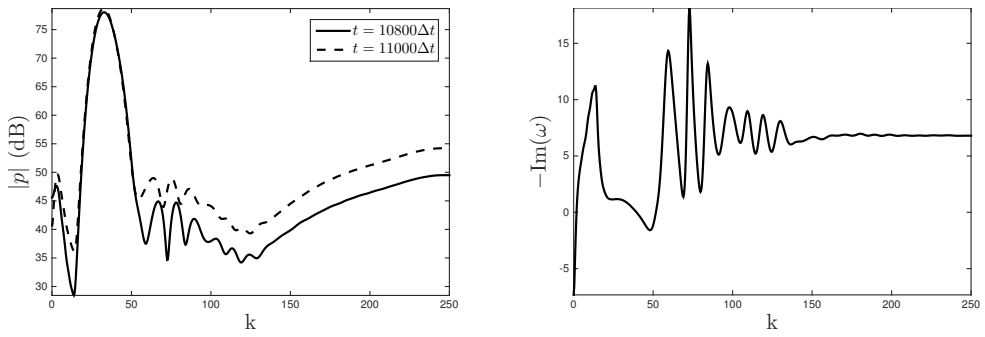

(a) (b)

Figure 5: Power spectrum of pressure fluctuations at two times (a) and the corresponding growth rate of the pressure (b).

above, it is conjectured that the behavior of aliasing is purely related to the numerical implementation and should arise independently of the physical problem under consideration.

For a range of wavenumbers, the eigenvalue problem, Eq. (8), is solved to form the dispersion relation, $D(\omega, k) = 0$, of the discrete problem. For each wavenumber considered, the numerical dispersion relation gives a range of numerical frequencies, ω, of which some can be identified as physical modes and all others are spurious, or unphysical modes. From these modes, it is possible to analyze the error or the stability of the problem. Only the unstable modes are of interest in this work and they must be separated from the stable modes. To achieve this, only the modes with the smallest imaginary part of ω, *i.e.* the most unstable modes, are stored.

In Figure 6a the most unstable mode is shown for each wavenumber and a range of polynomial orders. As the polynomial order increases from $p = 1$ to $p = 5$, for a range of wavenumbers the growth rate converges to what appears to be the shape of a physical instability. This is further evidenced by calculating the group velocity, $\mathrm{Re}\left(\frac{\mathrm{d}\omega}{\mathrm{dk}}\right)$, from Figure 6b. For the range of wavenumbers from $k = 0$ to $k = 5$ and polynomial orders 3 to 5, the group velocity is calculated from the slope of the dashed line. The group velocity indicates that the physical unstable mode is convected downstream at a velocity of 0.25, which is expected as it is the velocity at the center of the shear layer.

As the polynomial order increases, it is clear that the growth rate of the most unstable mode increases significantly over the range of wavenumbers considered and becomes less physical. The group velocity of these modes is equal to, or nearly, zero for a wide range of wavenumbers. Zero group velocity explains why aliasing instabilities pollute the solution; they build up over the integration time and are not convected out of the domain. These behaviors are in agreement with the aliasing instabilities seen in the duct radiation problem above. Namely, the polynomial order strongly impacts

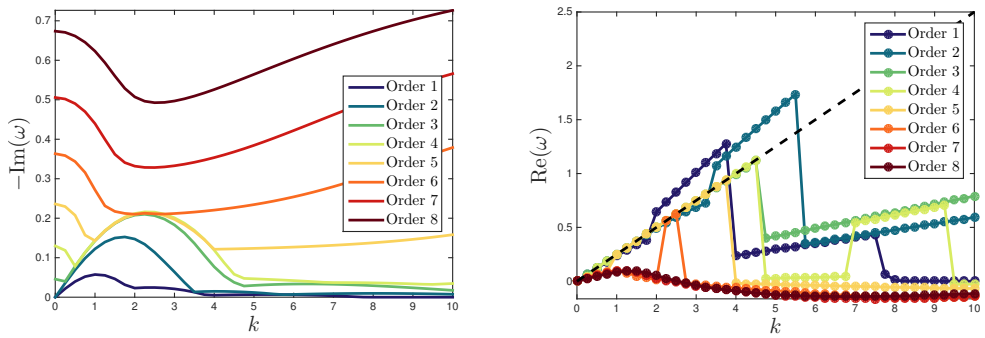

(a) (b)

Figure 6: Growth rates of the most unstable mode for a range of polynomial orders (a) and the real part of the numerical frequency of the modes (b).

the aliasing and the aliasing instabilities are mostly absolute instabilities that do not convect out of the domain. While the dispersion analysis indicates that there may be a range of wavenumbers at which the unphysical modes do not dominate, in practical problems however, a wide range of wavenumbers will be present and are likely to excite the unphysical modes.

5. Summary and conclusions

Instabilities driven by aliasing in solutions to the LEE in the time domain with the DGM have been characterized. A model exhaust noise problem with a shear layer was used to show the onset of aliasing instabilities in practical computations. The spectral properties of the aliasing instabilities were studied by using a new fully-discrete dispersion analysis technique for the LEE DGM. Effect of the polynomial order of the scheme on the growth of these instabilities was shown. The results of this study indicate that aliasing errors are largely absolute instabilities which build up in the solution over time and are highly sensitive to the polynomial order.

Future work will involve the development of filters to specifically target aliasing. The dispersion analysis will be used to develop *a priori* indicators of regions of the mean flow prone to aliasing and where filtering is most necessary. The impact of the accuracy of the mean flow representation on the solution will also be studied.

Acknowledgments

This work is performed as part of the CRANE (Community and Ramp Aircraft NoisE) project and is supported in full by European Union funding under the Framework Programme 7.

REFERENCES

1. H. L. Atkins and C.-W. Shu, "Quadrature-Free Implementation Of The Discontinuous Galerkin Method For Hyperbolic Equations," Tech. Rep. 96-51, NASA Langley Research Center, Hampton, Virginia, Aug. 1996.
2. D. Stanescu, M. Y. Hussaini, and F. Farassat, "Aircraft engine noise scattering by fuselage and wings: a computational approach," *Journal of sound and vibration*, vol. 263, no. 2, pp. 319–333, 2003.
3. M. Bernacki and S. Piperno, "A dissipation-free time-domain discontinuous Galerkin method applied to three-dimensional linearized Euler equations around a steady-state non-uniform inviscid flow," *Journal of Computational Acoustics*, vol. 14, no. 04, pp. 445–467, 2006.
4. R. Della Ratta Rinaldi, A. Iob, and R. Arina, "An efficient discontinuous Galerkin method for aeroacoustic propagation," *International Journal for Numerical Methods in Fluids*, vol. 69, pp. 1473–1495, July 2012.
5. J. S. Hesthaven, *Spectral methods for time-dependent problems*. No. 21 in Cambridge monographs on applied and computational mathematics, Cambridge ; New York: Cambridge University Press, 2007.
6. M. E. Goldstein, "An exact form of Lilley's equation with a velocity quadrupole/temperature dipole source term," *Journal of Fluid Mechanics*, vol. 443, pp. 231–236, 2001.
7. K. Hamiche, G. Gabard, and H. Bériot, "A higher-order finite element method for the linearised Euler equations.," 2014.
8. J. Berland, C. Bogey, and C. Bailly, "Low-dissipation and low-dispersion fourth-order Runge–Kutta algorithm," *Computers & Fluids*, vol. 35, pp. 1459–1463, Dec. 2006.
9. J. S. Hesthaven, *Nodal discontinuous Galerkin methods: algorithms, analysis, and applications*. No. 54 in Texts in applied mathematics, New York: Springer, 2008.
10. F. Q. Hu, M. Hussaini, and P. Rasetarinera, "An Analysis of the Discontinuous Galerkin Method for Wave Propagation Problems," *Journal of Computational Physics*, vol. 151, pp. 921–946, May 1999.
11. G. Gabard and E. Brambley, "A full discrete dispersion analysis of time-domain simulations of acoustic liners with flow," *Journal of Computational Physics*, vol. 273, pp. 310–326, Sept. 2014.
12. G. Gabard and R. J. Astley, "Theoretical model for sound radiation from annular jet pipes: far- and near-field solutions," *Journal of Fluid Mechanics*, vol. 549, p. 315, Feb. 2006.